AGU PUBLICATIONS

Geophysical Research Letters

RESEARCH LETTER
10.1002/2017GL073629

Special Section:
Early Results: Juno at Jupiter

Key Points:
- Uncertainty on Jupiter's low-degree gravity moments due to differential rotation is larger than the Juno measurement uncertainty
- This study provides the maximal possible contribution to J_2, J_4, J_6, and J_8 due to differential rotation
- Most of Jupiter's internal models do not match Juno's gravity values, but accounting for differential rotation provides possible solutions

Correspondence to:
Y. Kaspi,
yohai.kaspi@weizmann.ac.il

Citation:
Kaspi, Y., et al. (2017), The effect of differential rotation on Jupiter's low-degree even gravity moments, *Geophys. Res. Lett.*, *44*, 5960–5968, doi:10.1002/2017GL073629.

Received 28 MAR 2017
Accepted 11 MAY 2017
Accepted article online 25 MAY 2017
Published online 19 JUN 2017

The effect of differential rotation on Jupiter's low-degree even gravity moments

Y. Kaspi[1], T. Guillot[2], E. Galanti[1], Y. Miguel[2], R. Helled[3], W. B. Hubbard[4], B. Militzer[5], S. M. Wahl[5], S. Levin[6], J. E. P. Connerney[7], and S. J. Bolton[8]

[1]Department of Earth and Planetary Sciences, Weizmann Institute of Science, Rehovot, Israel, [2]Université Côte d'Azur, OCA, CNRS, Nice, France, [3]Center for Theoretical Astrophysics and Cosmology, University of Zurich, Zurich, Switzerland, [4]Lunar and Planetary Laboratory, University of Arizona, Tucson, Arizona, USA, [5]Department of Earth and Planetary Science, University of California, Berkeley, California, USA, [6]Jet Propulsion Laboratory, Pasadena, California, USA, [7]NASA/GSFC, Greenbelt, Maryland, USA, [8]Southwest Research Institute, San Antonio, Texas, USA

Abstract The close-by orbits of the ongoing Juno mission allow measuring with unprecedented accuracy Jupiter's low-degree even gravity moments J_2, J_4, J_6, and J_8. These can be used to better determine Jupiter's internal density profile and constrain its core mass. Yet the largest unknown on these gravity moments comes from the effect of differential rotation, which gives a degree of freedom unaccounted for by internal structure models. Here considering a wide range of possible internal flow structures and dynamical considerations, we provide upper bounds to the effect of dynamics (differential rotation) on the low-degree gravity moments. In light of the recent Juno gravity measurements and their small uncertainties, this allows differentiating between the various models suggested for Jupiter's internal structure.

1. Introduction

The Juno spacecraft has been in orbit around Jupiter since July 2016 and has enabled measuring the gravity spectrum of Jupiter to an unprecedented accuracy. These measurements have two main objectives: First, to better constrain the internal density structure of Jupiter, which will be mostly obtained by improving the accuracy for the already known low-degree even gravity moments (J_2, J_4, J_6, and J_8). Second, atmospheric and interior dynamics (often referred to as differential rotation) can be better constrained by measurements of high-degree gravity moments, where the dynamical component of the gravity spectrum (ΔJ_n) dominates that of the solid-body (static) gravity spectrum [*Hubbard*, 1999; *Kaspi et al.*, 2010], and the odd gravity moments that are only caused by dynamical effects [*Kaspi*, 2013]. However, the two objectives are entangled together as the dynamics also affect the low-degree even moments, and this small dynamical contribution to the even low-degree moments cannot be separated from the static contribution.

Jupiter internal structure models use observational constrains such as radius, mass, and known low-degree even gravity moments to determine the density distribution within the planet. There has been much progress in recent years in the understanding of hydrogen-helium mixtures at high pressures [e.g., *Saumon and Guillot*, 2004; *Militzer*, 2006; *Fortney and Nettelmann*, 2010; *Militzer and Hubbard*, 2013; *Becker et al.*, 2014; *Militzer et al.*, 2016], which these models rely on for the internal structure calculations. Yet these models include only rigid rotation, the effect of which is entirely accounted for in the effective gravity potential. To leading order, the dynamical contribution to the low-degree even moments is much smaller than the static contribution, yet it may cause a discrepancy between the measured values and the model solutions. Up to the recent Juno gravity measurement this did not pose a difficulty on the internal structure models, since the uncertainty of the measured low-degree moments was much greater than the dynamical contribution to the gravity moments. However, as the Juno gravity measurements improved the accuracy by 2 orders of magnitude [*Bolton et al.*, 2017; *Folkner et al.*, 2017], compared to previous estimates based on Voyager and Cassini data [*Campbell and Synnott*, 1985; *Jacobson*, 2003], the dynamical contribution to the low-degree moments is now larger than the uncertainty. In addition, none of the currently published internal structure models [see *Miguel et al.*, 2016, and references therein] can match all four Juno-measured gravity moments, and since the discrepancies between

the internal structure model values and the measurements are of the same order of the dynamical contribution, differential rotation might be invoked to explain these discrepancies. The purpose of this paper is to explore the possible role of dynamics on the low-degree gravity moments.

Better constraining the internal structure models has important consequences, as it allows for better determination of Jupiter's core mass and total mass of heavy elements (all elements that are heavier than helium), which is crucial to understand the formation of the planet [e.g., *Guillot*, 1999; *Hubbard et al.*, 2002; *Helled et al.*, 2014; *Militzer et al.*, 2016]. Both quantities have large uncertainties, with values ranging from 0 to 10 Earth masses ($M_\oplus$) for the core mass, and 10 to about 40 $M_\oplus$ for the total mass of heavy elements within the planet [e.g., *Saumon and Guillot*, 2004; *Nettelmann et al.*, 2008; *Militzer et al.*, 2008; *Nettelmann et al.*, 2012; *Hubbard and Militzer*, 2016; *Miguel et al.*, 2016]. Juno's accurate measurement of Jupiter's gravitational moments, J_n, is fundamental to better constrain these quantities. However, this also requires better constraining the dynamical contribution to the gravity moments, ΔJ_n [*Guillot*, 1999; *Guillot et al.*, 2004].

This study aims at providing an upper bound for the influence of differential rotation on the low-degree even gravitational moments. Therefore, we explore a wide possible range of internal flows. The only knowledge we have about the flow patterns are the observed flows at the planet's cloud level [e.g., *Porco et al.*, 2003]. Those show a pattern of multiple east-west jet streams which penetrate to an unknown depth beneath the condensable cloud level. One of the prime goals of the Juno mission is to try and determine the depth of these flows, an objective which might be best achieved using the measured odd gravity spectrum [*Kaspi*, 2013]. Yet there is also a possibility that beneath this layer, there are deep flow structures that might be completely decoupled from the observed cloud level winds [*Galanti and Kaspi*, 2017]. If these structures are large scale, as shown in some internal convection 3-D hydrodynamical models [e.g., *Aurnou and Olson*, 2001; *Christensen*, 2002; *Heimpel et al.*, 2005; *Kaspi et al.*, 2009; *Gastine and Wicht*, 2012], they may have a nonnegligible effect on the low-degree gravity moments. Therefore, even if the depth of the observed cloud level flow will be determined by analysis of the high-degree or odd gravity spectrum, it is still possible that deep equatorially symmetric internal flow structures with significant mass will contribute to the low-degree gravity spectrum.

In section 2 we discuss the methods by which we calculate the dynamical contribution to the gravity field and how it is implemented. Section 3 shows the dynamical contribution to the low-degree gravity moments for this wide range of possible velocity profiles, and section 4 analyzes how this compares to the difference between the recent Juno measured values, their uncertainties, and interior structure models. We conclude in section 5.

2. Methods

Calculating the dynamical contribution to the gravity moments $\left(\Delta J_n\right)$ relies on the relationship between density gradients and the flow field. For a rapidly rotating planet (small Rossby number) the dynamics are to leading order geostrophic, meaning the dynamically induced pressure gradients are in balance with the Coriolis force. This also implies that the dynamically induced density perturbations are balanced by the flow and can be related through thermal wind balance, namely

$$2\mathbf{\Omega}\cdot\nabla(\tilde{\rho}\mathbf{u})=\nabla\rho'\times\mathbf{g}, \tag{1}$$

where $\mathbf{\Omega}$ is the rotation rate of the planet, 1.76×10^{-4} s^{-1}, $\tilde{\rho}$ is the static radial density distribution, $\mathbf{u}$ is the 3-D velocity field, ρ' is the density deviation due to dynamics and $\mathbf{g}$ is the radial gravity field obtained by integrating $\tilde{\rho}$ [*Pedlosky*, 1987; *Kaspi et al.*, 2009]. Here density variations related to the oblate shape of the planet have been ignored. It has been suggested that oblateness effects, such as the effect of oblateness on the background density state $\tilde{\rho}(r,\theta)$ [*Cao and Stevenson*, 2017a] and the deviations from the mean radial gravity $g'(r,\theta)$ induced by the flow itself [*Zhang et al.*, 2015], might be important for the gravity moments. However, solving self-consistently for the full oblate system, *Galanti et al.* [2017] have shown that these oblateness effects give only a small contribution to the gravity moments, meaning that equation (1) captures well the leading order balance.

The rapid rotation of the planet implies that angular momentum conservation constrains the leading order zonal flow to be aligned parallel to the axis of rotation [*Kaspi et al.*, 2009; *Schneider and Liu*, 2009]. If the fluid would have been completely barotropic, this would result in the zonal flow being constant along the direction of the spin axis [e.g., *Busse*, 1976; *Hubbard*, 1999]. However, the alignment with the axis of rotation does not

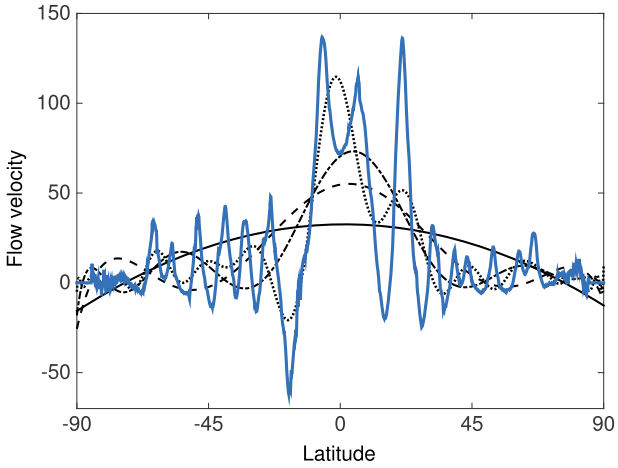

Figure 1. Examples of the explored latitudinal profiles of the flow (ms^{-1}), ranging from smoothed profiles representing possible internal flows (black) to the observed surface winds (blue). Shown in black are the polynomial fits up to degree 2 (solid), 6 (dashed), 10 (dash-dotted), and 30 (dotted). All profiles have been extended along the direction of the spin axis over a range of decay depths ranging from shallow flows with an exponential decay of $H = 100$ km (~15 bars), to fully barotropic flows constant along the direction of the spin axis. The nonzero values at the poles determined by the polynomial fits have very little effect on the results since the polar regions contain only a small fraction of the planetary mass.

exclude baroclinic flows, where the flow velocity decays along the direction of the spin axis, as has been suggested due to magnetic Ohmic dissipation [*Liu et al.*, 2008; *Cao and Stevenson*, 2017b], or due to the high density in the interior [*Kaspi et al.*, 2009]. Therefore, to account for the widest possible range of vertical flow structures, we consider flow fields with a varying exponential decay parameter (H). When H is comparable to the radius of the planet, the flow is very deep (nearly constant along the direction of the spin axis), while when H is smaller it sets the e-folding decay depth of the flow.

Given such an assumed flow profile, and using the background mean density ($\tilde{\rho}$) from *Wahl et al.* [2017], integrating the azimuthal component of equation (1) gives

$$\rho'(r,\theta) = \frac{2\Omega r}{g}\int^{\theta}\frac{\partial}{\partial z}\left(\tilde{\rho}u\left(r,\theta'\right)\right)\mathrm{d}\theta' + \rho'_0(r), \tag{2}$$

where $u(r,\theta)$ is the zonal (east-west) component of the flow, which depends on radius (r) and latitude (θ), z denotes the direction of the axis of rotation, and ρ'_0 is an unknown function of radius coming from the integration. Although the density ρ' cannot be determined uniquely due to the unknown ρ'_0, the gravity moments due to dynamics

$$\Delta J_n = -\frac{2\pi}{Ma^n}\int_{-1}^{1}\mathrm{d}\mu\int_0^a r^{n+2}P_n(\mu)\rho'(r,\mu)\,\mathrm{d}r, \tag{3}$$

can be determined uniquely since

$$\int_{-1}^{1}\mathrm{d}\mu\int_0^a r^{n+2}P_n(\mu)\rho'_0(r)\mathrm{d}r = 0. \tag{4}$$

Here M is the planetary mass, a is the mean radius, P_n is the n-th degree Legendre polynomial, and $\mu = \cos\theta$. Therefore, given an assumed flow profile, the resulting dynamical gravity moments can be determined.

Previous studies have used equation (2) given a prescribed zonal wind field obtained from the observed surface winds with an e-folding depth H [e.g., *Kaspi et al.*, 2010; *Kaspi*, 2013; *Kong et al.*, 2013]. However, as it is possible that in addition to the observed surface flows there exist deep structures differentially rotating with significant masses due to the high density at depth, we also allow for a wide range of latitudinal profiles that are different than the observed cloud level wind profile (Figure 1, blue). Since the interior profile is unknown, we simply used smoothed profiles of the upper level flows, obtained by matching the observed cloud level profile to a series of polynomial fits ranging from degrees 2 to 30 (Figure 1, black). Obviously, this set of latitudinal structures is only a subset of the possible flow fields in the interior, yet we find that it contains a wide set of solutions and adding more possible latitudinal profiles does not change the overall picture. Since we are only considering the low-degree even moments, only the north-south symmetric part of the flow contributes to the solution. Note that since we are only interested in the low-degree harmonics, rapid latitudinal variations in the velocity profile (as seen in the observed cloud-level wind), have a very small effect on the results. This can be seen in Figure 2 showing the ratio between the dynamical gravity moments and the static values for J_2, J_4, J_6, and J_8, as a function of the polynomial degree and exponential decay depth of the flow. It shows that the ratio for these low-degree moments asymptotes to nearly constant values as the polynomial degree becomes high.

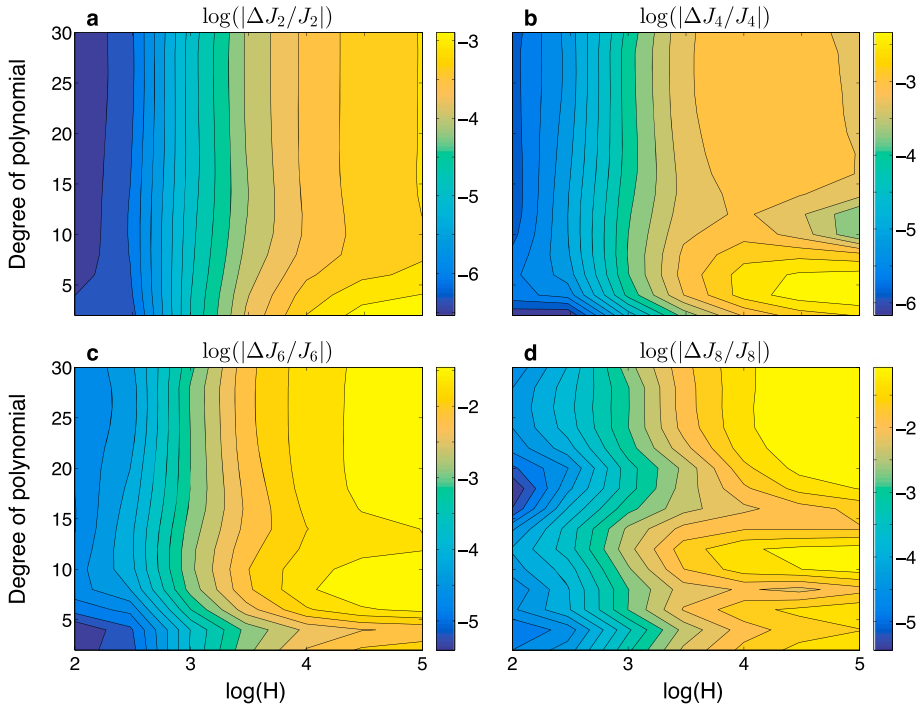

Figure 2. Logarithm of the ratio between the dynamical gravity moments and the static values $\left(\Delta J_n/J_n\right)$ for (a) J_2, (b) J_4, (c) J_6, and (d) J_8, as a function of the polynomial degree fit to the observed cloud level wind and the *e*-folding decay depth of the flow (*H*, in km).

3. The Dynamical Contribution to the Even Gravity Moments

Using smoothed profiles of the differential rotation potential derived from the Voyager measured wind profile, *Hubbard* [1982] calculated the ratio of the dynamical induced gravity harmonics to the J_n measured by Voyager, considering barotropic flows along cylinders. Thus, those solutions are specific solutions to the more general cases shown here and correspond to the lower right corner of each of the panels in Figure 2. He found that $\Delta J_n/J_n$ for even moments 2–8 are roughly 0.001, 0.006, 0.02, and 0.01, respectively, and those values match well the corresponding values in Figure 2. For J_2 and J_4, as expected, the largest values in Figure 2 are found for the low polynomial degrees 2 and 4, where the flow field projects most strongly on the low-degree moments. For J_6 and J_8, where the structure becomes more complex, there is also strong contribution from higher polynomials (Figures 2c and 2d)

The corresponding values in the phase planes of J_2/J_4, J_4/J_6, and J_6/J_8 are shown in Figure 3. It is found that when *H* is small (very little mass is involved in the flow) all solutions cluster around zero, and only when *H* becomes large enough ($H > 1000$ km) then ΔJ_n values become distinguishable in Figure 3. The sign of ΔJ_2, ΔJ_4, and ΔJ_6 are mostly positive, negative, and positive, respectively, reflecting the projection of the density anomaly resulting from the shape shown in Figure 1 on P_n and taking into account the minus sign in equation (3). As *H* becomes larger, more mass is involved in the flow and the scatter of ΔJ_n due to the different wind profiles becomes bigger. We also see that the lowest-order polynomial projections (circles and diamonds in Figure 3) tend to yield the largest contributions, especially on ΔJ_2, and ΔJ_4. As discussed earlier, this only represents a small subset of the possible flow fields, but other flow patterns give results within the same range [e.g., *Dowling*, 1995; *Kong et al.*, 2016], and therefore, the spread in Figure 3 gives a good sense for the range of possible ΔJ_n.

The significance of the range of possible ΔJ_n values shown in Figure 3 can be evaluated when compared to the uncertainty of the measured full J_n, which include both the bigger static effect (due to the planetary shape and interior density distribution) and the smaller dynamical effect. Initial Juno results from the first two perijoves show that the measured gravity values are $J_2 = 14,696.51 \pm 0.27 \times 10^{-6}$, $J_4 = -586.62 \pm 0.36 \times 10^{-6}$, $J_6 = 34.24 \pm 0.24 \times 10^{-6}$, and $J_8 = -2.50 \pm 0.31 \times 10^{-6}$ [*Folkner et al.*, 2017]. Thus, given the range of values

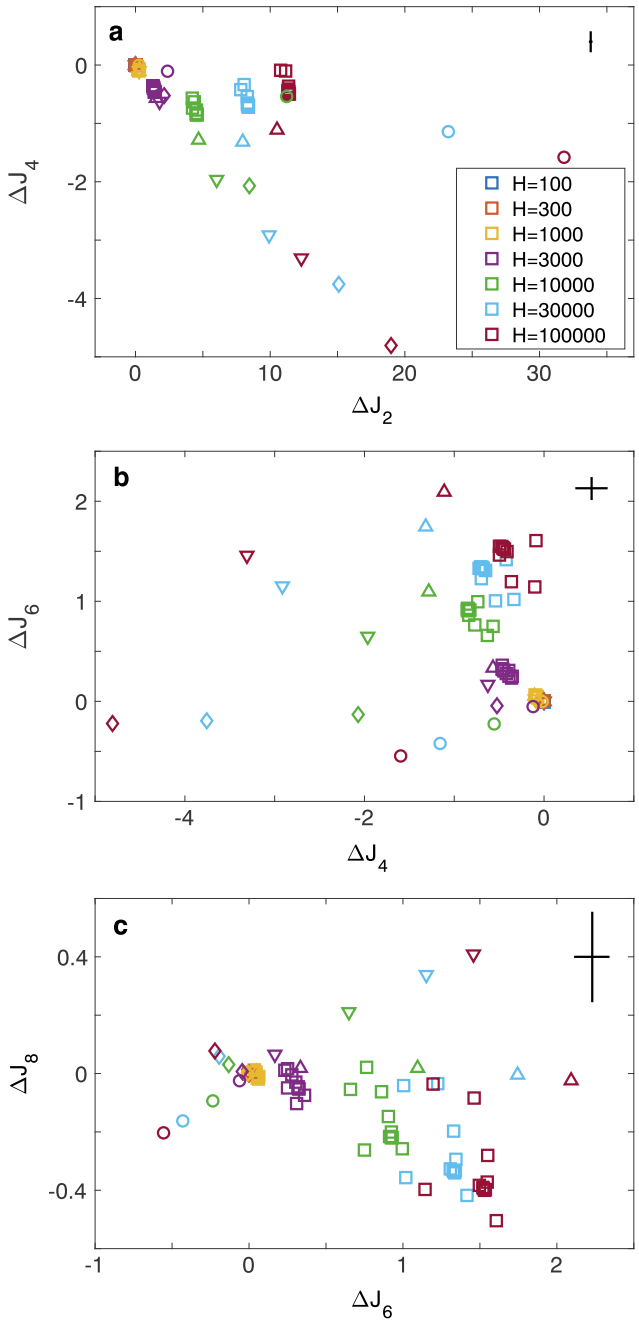

Figure 3. (a–c) Scatter plots of the gravity moments ($\times 10^6$) for different differential rotation scenarios. Colors represent the exponential decay depth (in km, see legend). Zonal flows range from very smoothed latitudinal structures to flows more similar to the observed surface zonal winds (Figure 1). The lowest-order polynomial fits to the latitudinal wind profile (2nd, 4th, 6th, and 8th order) are marked as circles, diamonds, downward pointing triangles, and upward pointing triangles, respectively. Higher-order polynomial fits are marked with squares. The magnitude of the current Juno-measured uncertainty is marked by the black crosses in the upper right corner of each panel.

in Figure 3, the possible range of values of ΔJ_n for all four moments are much larger than the uncertainty in J_n (crosses in Figure 3), by a factor 120 for J_2, 14 for J_4, 11 for J_6, and 3 for J_8, meaning that the low-degree ΔJ_n can have a significant effect on the measurement. Of course, these values are the largest ones obtained for zonal winds with very large H, extending very deep to the interior of the planet, a situation that is likely unrealistic (although deep large-scale flow structures that are decoupled from the upper level flow may exist). But even for smaller H values, the values in most cases shown are larger than the Juno uncertainty, meaning that the possible range of ΔJ_n must be considered as uncertainties for interior models. This had been shown to be the case already with the Voyager measurements, where the effect could be approximated by slightly increasing the J_4 error bar [*Guillot*, 1999]. The error on J_2 from differential rotation is in fact larger; however, it can be easily corrected for by a slight change in core mass and heavy elements abundance [*Guillot*, 1999]. Now that the measurement uncertainty is so small, as shown in Figure 4, the contribution of differential rotation must be taken into account to interpret Juno data in terms of constraints for the interior models.

4. Implications for Interior Structure Models

Constraints on Jupiter's gravity field to date have been relatively uncertain and variable, as shown in Figure 4a. As a result, models of Jupiter's interior have so far effectively been constrained by the measurements of the planet's mass, rotation period, radius, and only two gravitational moments, J_2 and J_4. The situation has changed with the recent measurements from the Juno spacecraft, resolving the ambiguous J_4 and J_6 values, and both J_6 and J_8 can potentially be used now to constrain new interior models [*Wahl et al.*, 2017]. Figure 4a also shows a series of pre-Juno interior model solutions from *Miguel et al.* [2016] fitting the planet's radius and J_2, but more loosely J_4 and J_6. These models assume that the interior is split in three distinct, homogeneous layers: a dense core, a helium-rich metallic envelope, and a helium-poor molecular envelope.

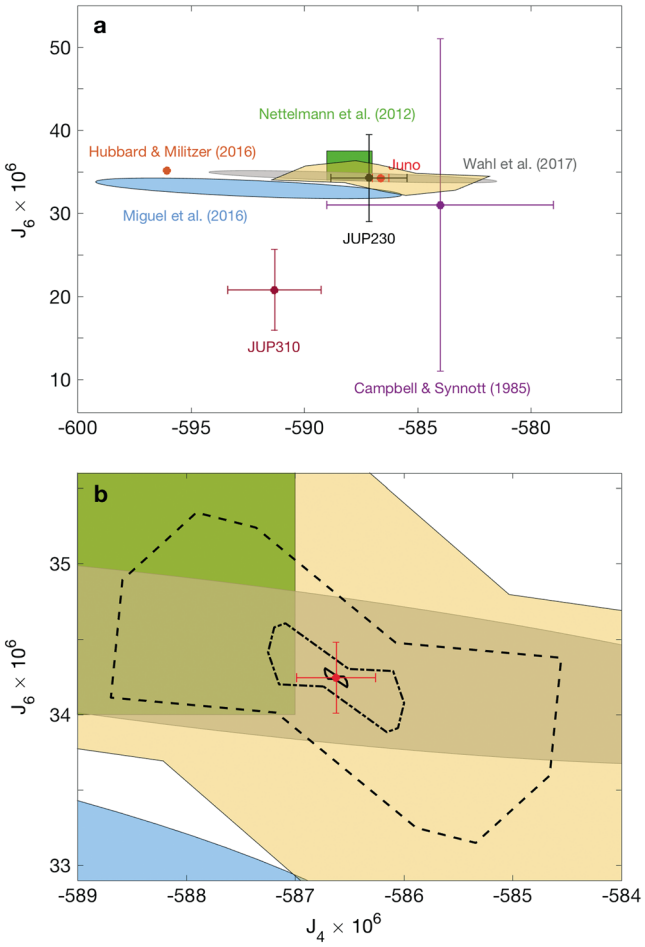

Figure 4. (a) Historical (pre-Juno) observed values of J_4 and J_6 by *Campbell and Synnott* [1985] (purple), by *Jacobson* [2003] (black), and *Jacobson* [2009] (maroon) compared to Juno's measurement from the first two orbits (red). Interior model solutions are shown for the models of *Nettelmann et al.* [2012] (green), *Hubbard and Militzer* [2016] (orange), *Miguel et al.* [2016] (blue), and *Wahl et al.* [2017] (gray), and overlying centered around the Juno-measured values are the range of solutions possible due to dynamics $(J_n - \Delta J_n)$ (transparent yellow). (b) A blowup of the central region of Figure 4a. Contours show different H values with $H = 1000$ km (solid), $H = 3000$ km (dash-dotted), and $H = 10,000$ km (dashed).

Solutions with a relatively low-density equation of state (EOS) [*Saumon et al.*, 1995; *Becker et al.*, 2014] require more heavy elements in the planetary interior and thus allow for a larger range of solutions. Solutions with a higher-density EOS [*Militzer and Hubbard*, 2013] allow for comparatively fewer solutions. With the former EOSs, when accounting for uncertainties in the calculation of gravitational moments, the range of solutions from both *Nettelmann et al.* [2012] and *Miguel et al.* [2016] can be considered as compatible with the Juno gravitational moments. With the latter EOS, the value of J_4 remains significantly lower than the Juno measurement with a three-layer model [see *Hubbard and Militzer*, 2016; *Miguel et al.*, 2016]. However, using the more elaborate concentric Maclaurin spheroid method [*Hubbard*, 2012, 2013], with the same EOS allows getting solutions which are compatible with the Juno measurements even if the effect of differential rotation is small [*Wahl et al.*, 2017].

Thus, at face value, the very small uncertainty of the Juno measurements would imply either very tight constraints on the core mass and total mass of heavy elements for the first series of EOSs or a requirement of more complex structure models with more layers and/or nonadiabatic layers [e.g., *Leconte and Chabrier*, 2012; *Vazan et al.*, 2016; *Helled and Stevenson*, 2017]. However, the contribution of differential rotation may not be negligible, implying that a wide range of internal structure models must be considered. Since the measured values of J_n are composed of the sum of the static and dynamic values, this can be estimated simply by accounting for the dynamical values found in Figure 3 and reporting them in Figure 4 (yellow transparent shading). This range, showing that the values are big enough to account for the difference between the measurements and the interior structure models, has been obtained by subtracting the maximal values of the range shown in Figure 3b from the measured Juno values of J_4 and J_6. The values are subtracted since we are interested in the values that can cover the difference between the measurements and the interior models. However, in the flow profiles considered in Figure 3, we took only the polynomial fits to the observed cloud level winds, which are all characterized by an eastward flow around the equator due to the observed cloud level superrotation. Considering though that the flow patters we use come also to represent possible large-scale flows beneath the cloud level flow, which a priori can be completely decoupled from the cloud level winds [*Galanti and Kaspi*, 2017], we also include the same flow patterns with opposite values (i.e., large-scale westward flow near the equator). In these cases the H values still represent the exponential decay depth but for a flow structure that begins underneath the superficial cloud level flow. Since we are only interested in the flow that is the most influential on the gravity field, we do not go into the details of having the superficial cloud level flows above the deeper (more massive) flow structures, and simply take the

same flow patterns (as shown in Figure 1) with a negative sign. This gives a very broad range of possible flow patterns, which we consider to be a big enough representation of the all-possible flow patterns. This results in the dynamical contribution that is to the left of the measured J_4/J_6 point in Figure 4, while the positive equatorial flow values are the part of the yellow shading that is to the right of the measured J_4/J_6 point. Note that the solutions taking into account the positive and negative winds do not converge exactly at the measured Juno J_4/J_6 point, as would be implied from Figure 3, because we allow for some margin around the Juno J_4/J_6 point, coming from different possible wind profiles.

Overall, the dynamical range of ΔJ_4 is about 8×10^{-6} and that of ΔJ_6 about 4×10^{-6}, which is much larger than the uncertainty in the measurement of 0.36×10^{-6} and 0.24×10^{-6} for the two moments, respectively. Figure 4a shows that the dynamical range allows a significant fraction of the solutions of *Nettelmann et al.* [2012] to be compatible with the Juno constraints, and when accounting for uncertainties in the calculation of gravitational moments (about 2×10^{-6} in J_6) in *Miguel et al.* [2016] (see their Figure 6), a major part of these solutions are also compatible with the Juno constraints. This implies that without another constraint on the extent of differential rotation, the improvement on our determination of the core mass and total mass of heavy elements in Jupiter may be limited. Note however that the *Hubbard and Militzer* [2016] solution is still far from the measured J_4 values. Solutions with that EOS therefore require interior structure models beyond the traditional three-layer models as used by *Wahl et al.* [2017].

The large uncertainty due to the dynamical contribution in Figure 4a corresponds to the most extreme cases of very large H values and flow patterns that are not varying much with latitude (thus have a large projection on J_4 and J_6). Focusing on more realistic values of H (Figure 4b), reduces the uncertainty considerably. The $H = 1000$ km contour is within the measurement uncertainty and the $H = 3000$ km is just larger than it. Note, however, that the Galileo probe-measured wind speeds that are twice the value of the surface winds extending down to 22 bar [*Atkinson et al.*, 1996]. Although unlikely, if such wind speeds extend to the depths considered in this study, then we find that the range of dynamical ΔJ_n grows nearly linearly with the wind velocity, implying ΔJ_4 and ΔJ_6 of about 2×10^{-6} and 1×10^{-6}, respectively, for the $H = 3000$ km case. It is obvious from these solutions that the effect of H is much more important than the effect of the specific latitudinal structure of the flow (Figure 1). Furthermore, most of the interior model solutions have J_4 values below the Juno measurement, which would require a deep interior flow that is in the opposite direction relative to the observed upper level zonal wind, i.e., a subrotating low-latitude flow beneath the superficial superrotating flow. Based on the values of J_4 in their calculation *Militzer et al.* [2008] reached a similar conclusion.

5. Conclusions

Jupiter's measured gravity moments have a contribution from both the static (internal structure and planetary shape) and dynamic (flow relative to the solid-body rotating planet) components. The dynamical contribution for the low-degree even gravity moments J_2, J_4, J_6, and J_8 is generally at least 1–3 orders of magnitude smaller than the static contribution (Figure 2). Yet the precision of the recent Juno measurements is such that the uncertainty on the measurements is even smaller than the dynamical gravity moments. Thus, it is crucial to estimate the dynamic contribution to the even J_n; otherwise, most internal structure models have to be ruled out as they do not fit within the very small uncertainty of the Juno measurements. The dynamical contribution therefore gives now the effective uncertainty on the low-degree even J_n for internal structure models using different EOSs and calculating the core mass, heavy element distribution, and density structure [e.g., *Nettelmann et al.*, 2012; *Miguel et al.*, 2016; *Lozovsky et al.*, 2017; *Wahl et al.*, 2017]. This study allows differentiating between these internal structure models in terms of their consistency with the Juno measurements and provides information on the structure and magnitude of the differential rotation needed to match the different internal structure models.

To further narrow down the range of internal structure models, more information about the differential rotation will be needed. This information can come from further Juno measurements of the odd (J_3, J_5, J_7, etc.) and high-degree even (J_{10}, J_{12}, and J_{14}) gravity moments. The odd gravity moments, which have no contribution from the static component and are therefore a pure sign of dynamics [*Kaspi*, 2013], can give information particularly about the depth of the atmospheric flows, where we know already from observations of the cloud level flow that there exists a north-south asymmetry (meaning nonzero odd gravity moments). Constraining in such a way the depth of the dynamical atmosphere will give also the values for J_2, J_4, J_6, and J_8 coming

from the upper level flows. Nonetheless, this cannot completely constrain the lower-degree even ΔJ_n since it is possible that there is an even ΔJ_n contribution coming from internal flows that are decoupled from the upper level flows and without any north-south asymmetry. Further information about the overall flow and differential rotation within the planet can come also from the high-degree even gravity moments, particularly moments beyond J_{10}, where the dynamic contribution is greater than the static one [*Hubbard*, 1999; *Kaspi et al.*, 2010], that will likely be better resolved with more Juno orbits [*Folkner et al.*, 2017].

In summary, now, following the Juno measurements, when the uncertainties on the low-order zonal moments have become so small, the differential rotation question and the internal structure questions became entangled together. As the Juno mission progresses it is likely that further constraints on the differential rotation will enable narrowing the range of internal structures even more and provide information about the core mass, heavy element concentration, and density distribution. If the dynamics turn out to be only shallow, this will narrow down significantly the range of possible internal structure models, and those will need to be very specific in order to match observations. If the dynamics are deep, a wider range of models will be possible, making it harder to quantify exactly the properties of Jupiter's interior.

Acknowledgments
We thank the Juno Interiors Working Group for very helpful discussions. E.G. and Y.K. acknowledge support from the Israeli Ministry of Science, the Minerva foundation with funding from the Federal German Ministry of Education and Research and the Helen Kimmel Center for Planetary Science at the Weizmann Institute of Science. T.G. and Y.M. acknowledge support from CNES. R.H. acknowledges support from the Israeli Ministry of Science, and the BSF. B.M. and S.M.W. acknowledge support from the NSF. All authors acknowledge support from the Juno project.

References

Atkinson, D. H., J. B. Pollack, and A. Seiff (1996), Galileo Doppler measurements of the deep zonal winds at Jupiter, *Science*, *272*, 842–843.
Aurnou, J. M., and P. L. Olson (2001), Strong zonal winds from thermal convection in a rotating spherical shell, *Geophys. Res. Lett.*, *28*, 2557–2559, doi:10.1029/2000GL012474.
Becker, A., W. Lorenzen, J. J. Fortney, N. Nettelmann, M. Schöttler, and R. Redmer (2014), Ab initio equations of state for hydrogen (H-REOS.3) and helium (He-REOS.3) and their implications for the interior of Brown Dwarfs, *Astrophys. J. Suppl. Ser.*, *215*, 21.
Bolton, S. J., A. Adriani, V. Adumitroaie, J. Anderson, and the Juno Science Team (2017), Jupiter's interior and deep atmosphere: The initial pole-to-pole passes with the Juno spacecraft, *Science*, doi:10.1126/science.aal2108, in press.
Busse, F. H. (1976), A simple model of convection in the Jovian atmosphere, *Icarus*, *29*, 255–260.
Campbell, J. K., and S. P. Synnott (1985), Gravity field of the Jovian system from pioneer and Voyager tracking data, *Astrophys. J.*, *90*, 364–372.
Cao, H., and D. J. Stevenson (2017a), Gravity and zonal flows of giant planets: From the Euler equation to the thermal wind equation, *J. Geophys. Res. Planets*, *122*, 686–700, doi:10.1002/2017JE005272.
Cao, H., and D. J. Stevenson (2017b), Zonal flow magnetic field interaction in the semi-conducting region of giant planets, *Icarus*, submitted.
Christensen, U. R. (2002), Zonal flow driven by strongly supercritical convection in rotating spherical shells, *J. Fluid Mech.*, *470*, 115–133.
Dowling, T. E. (1995), Estimate of Jupiter's deep zonal-wind profile from Shoemaker-Levy 9 data and Arnold's second stability criterion, *Icarus*, *117*, 439–442.
Folkner, W., et al. (2017), Jupiter gravity field estimated from the first two Juno orbits, *Geophys. Res. Lett.*, doi:10.1002/2017GL073140, in press.
Fortney, J. J., and N. Nettelmann (2010), The interior structure, composition, and evolution of giant planets, *Space Sci. Rev.*, *152*, 423–447.
Galanti, E., and Y. Kaspi (2017), Deciphering Jupiters deep flow dynamics using the upcoming Juno gravity measurements and an adjoint based dynamical model, *Icarus*, *286*, 46–55.
Galanti, E., Y. Kaspi, and E. Tziperman (2017), A full, self-consistent, treatment of thermal wind balance on fluid planets, *J. Fluid Mech.*, *810*, 175–195.
Gastine, T., and J. Wicht (2012), Effects of compressibility on driving zonal flow in gas giants, *Icarus*, *219*, 428–442.
Guillot, T. (1999), A comparison of the interiors of Jupiter and Saturn, *Planet. Space Sci.*, *47*, 1183–1200.
Guillot, T., D. J. Stevenson, W. B. Hubbard, and D. Saumon (2004), The interior of Jupiter, in *Jupiter: The Planet, Satellites and Magnetosphere*, edited by F. Bagenal, T. E. Dowling, and W. McKinnon, pp. 35–57, Cambridge Univ. Press, Cambridge, U. K.
Heimpel, M., J. Aurnou, and J. Wicht (2005), Simulation of equatorial and high-latitude jets on Jupiter in a deep convection model, *Nature*, *438*, 193–196.
Helled, R., and D. Stevenson (2017), The fuzziness of giant planets' cores, *Astrophys. J. Lett.*, *840*, L4.
Helled, R., P. Bodenheimer, M. Podolak, A. Boley, F. Meru, S. Nayakshin, J. J. Fortney, L. Mayer, Y. Alibert, and A. P. Boss (2014), Giant planet formation, evolution, and internal structure, in *Protostars and Planets VI*, edited by H. Beuther et al., pp. 643–665, Univ. of Arizona Press, Tucson, Ariz.
Hubbard, W. B. (1982), Effects of differential rotation on the gravitational figures of Jupiter and Saturn, *Icarus*, *52*, 509–515.
Hubbard, W. B. (1999), Note: Gravitational signature of Jupiter's deep zonal flows, *Icarus*, *137*, 357–359.
Hubbard, W. B. (2012), High-precision Maclaurin-based models of rotating liquid planets, *Astrophys. J. Lett.*, *756*, L15.
Hubbard, W. B. (2013), Concentric Maclaurin spheroid models of rotating liquid planets, *Astrophys. J.*, *768*(1), 43.
Hubbard, W. B., and B. Militzer (2016), A preliminary Jupiter model, *Astrophys. J.*, *820*, 80.
Hubbard, W. B., A. Burrows, and J. I. Lunine (2002), Theory of giant planets, *Ann. Rev. Astron. Astrophy.*, *40*, 103–136.
Jacobson, R. A. (2003), JUP230 orbit solutions. [Availaable at http://ssd.jpl.nasa.gov/.]
Jacobson, R. A. (2009), Jupiter satellite ephemeris file Jup310, NASA Navigation and Ancillary Information Facility. [Available at https://naif.jpl.nasa.gov/pub/naif/generic-kernels/spk/satellites/jup310.cmt.]
Kaspi, Y. (2013), Inferring the depth of the zonal jets on Jupiter and Saturn from odd gravity harmonics, *Geophys. Res. Lett.*, *40*, 676–680, doi:10.1029/2012GL053873.
Kaspi, Y., G. R. Flierl, and A. P. Showman (2009), The deep wind structure of the giant planets: Results from an anelastic general circulation model, *Icarus*, *202*, 525–542.
Kaspi, Y., W. B. Hubbard, A. P. Showman, and G. R. Flierl (2010), Gravitational signature of Jupiter's internal dynamics, *Geophys. Res. Lett.*, *37*, L01204, doi:10.1029/2009GL041385.
Kong, D., X. Liao, K. Zhang, and G. Schubert (2013), Gravitational signature of rotationally distorted Jupiter caused by deep zonal winds, *Icarus*, *226*(2), 1425–1430.
Kong, D., K. Zhang, and G. Schubert (2016), A fully self-consistent multi-layered model of Jupiter, *Astrophys. J.*, *826*, 127.

Lozovsky, M., R. Helled, E. D. Rosenberg, and P. Bodenheimer (2017), Jupiter's formation and its primordial internal structure, *Astrophys. J.*, *836*(2), 16, doi:10.3847/1538-4357/836/2/227.
Leconte, J., and G. Chabrier (2012), A new vision of giant planet interiors: Impact of double diffusive convection, *Astron. Astrophys.*, *540*, A20.
Liu, J., P. M. Goldreich, and D. J. Stevenson (2008), Constraints on deep-seated zonal winds inside Jupiter and Saturn, *Icarus*, *196*, 653–664.
Miguel, Y., T. Guillot, and L. Fayon (2016), Jupiter internal structure: The effect of different equations of state, *Astron. Astrophys.*, *596*, A114.
Militzer, B. (2006), First principles calculations of shock compressed fluid helium, *Phys. Rev. Lett.*, *97*(17), 175501.
Militzer, B., and W. B. Hubbard (2013), Ab initio equation of state for hydrogen-helium mixtures with recalibration of the giant-planet mass-radius relation, *Astrophys. J.*, *774*, 148.
Militzer, B., W. B. Hubbard, J. Vorberger, I. Tamblyn, and S. A. Bonev (2008), A massive core in Jupiter predicted from first-principles simulations, *Astrophys. J.*, *688*, L45–L48.
Militzer, B., F. Soubiran, S. M. Wahl, and W. B. Hubbard (2016), Understanding Jupiter's interior, *J. Geophys. Res. Planets*, *121*, 1552–1572, doi:10.1002/2016JE005080.
Nettelmann, N., B. Holst, A. Kietzmann, M. French, R. Redmer, and D. Blaschke (2008), Ab initio equation of state data for hydrogen, helium, and water and the internal structure of Jupiter, *Astrophys. J.*, *683*, 1217–1228.
Nettelmann, N., A. Becker, B. Holst, and R. Redmer (2012), Jupiter models with improved ab initio hydrogen equation of state (H-REOS.2), *Astrophys. J.*, *750*, 52.
Pedlosky, J. (1987), *Geophysical Fluid Dynamics*, 710 pp., Springer, New York.
Porco, C. C., et al. (2003), Cassini imaging of Jupiter's atmosphere, satellites and rings, *Science*, *299*, 1541–1547.
Saumon, D., and T. Guillot (2004), Shock compression of deuterium and the interiors of Jupiter and Saturn, *Astrophys. J.*, *609*, 1170–1180.
Saumon, D., G. Chabrier, and H. M. van Horn (1995), An equation of state for low-mass stars and giant planets, *Astrophys. J.*, *99*, 713–741.
Schneider, T., and J. Liu (2009), Formation of jets and equatorial superrotation on Jupiter, *J. Atmos. Sci.*, *66*, 579–601.
Vazan, A., R. Helled, M. Podolak, and A. Kovetz (2016), The evolution and internal structure of Jupiter and Saturn with compositional gradients, *Astrophys. J.*, *829*, 118.
Wahl, S., et al. (2017), Comparing Jupiter interior structure models to Juno gravity measurements and the role of a dilute core, *Geophys. Res. Lett.*, doi:10.1002/2017GL073160, in press.
Zhang, K., D. Kong, and G. Schubert (2015), Thermal-gravitational wind equation for the wind-induced gravitational signature of giant gaseous planets: Mathematical derivation, numerical method and illustrative solutions, *Astrophys. J.*, *806*, 270–279.